Investigation of $AcXO_3$ (X = Al, Ga) perovskites for energy harvesting applications: a DFT approach

S. A. Aldaghfag[a], M. Ishfaq[b], Nasarullah[b], M. Yaseen[b,*]
[a]*Department of Physics, College of Sciences, Princess Nourah bint Abdulrahman University, P. O. Box 84428, Riyadh 11671, Saudi Arabia*
[b]*Spin-Optoelectronics and Ferro-Thermoelectric (SOFT) Materials and Devices Laboratory, Department of Physics, University of Agriculture, Faisalabad 38040, Pakistan*

Full potential linearized augmented plane wave (FP-LAPW) based computational study is presented for $AcAlO_3$ and $AcGaO_3$. Tolerance factor (τ_G) is 0.93 for $AcAlO_3$ and 0.90 for $AcGaO_3$ which reveal the stability of proposed perovskite oxides in cubic phase. The calculated band structures for both materials reveal the nonmagnetic semiconductive nature with energy band gaps of 3.98 and 2.75 eV for respective Al and Ga based perovskites. Total, and partial density of states (DOS) are computed for meaningful understanding of semiconducting behavior of the proposed perovskites. The partially filled O-2*p* and Ac-6*d* states are observed to lie in the vicinity of Fermi level. Furthermore, various parameters of optical spectra have also been computed to study the light matter interaction. Moreover, thermoelectric (TE) properties of both materials have been investigated by using semiclassical Boltzmann theory with constant relaxation time approximation. Calculated figure of merit (ZT) values for $AcAlO_3$ and $AcGaO_3$ are 0.23 and 0.20 at 800 K, respectively. Overall, computational study for titled perovskites indicate that these materials have application in UV sensors, photovoltaic and thermoelectric devices.

(Received December 3, 2023; Accepted April 4, 2024)

Keywords: Ab initio study, Perovskites; Semiconductors, Photovoltaic devices, Electronic properties, Optical properties, Thermoelectric devices

1. Introduction

Recurrent handling of environmental pollution and global energy crises has undoubtedly attracted researcher's interest for the development of new electrochemical energy storage devices and clean energy resources [1–3]. For this purpose, the exploration of new materials is one of the main forces accelerating current scientific development and technical innovation. Also, new materials with specific, improved, or innovative functionalities are essential for developing future technologies. Density functional theory (DFT) based theoretical modelling and simulating technology is considered as well developed and opening blueprints for investigating new materials to evaluate various physical characteristics of materials for the applications in innovative technologies [4-7].

Till up to date, much anticipated ABO_3 type perovskite oxides are the materials of exceptionally versatile class owing to their variety of physical properties and having flexibility to accommodate numerous cations of different sizes and plenty of oxygen atoms [8,9]. The benefits of perovskite oxides are found to be staggering with their reported power conversion efficiency (PCE) rising well above 20% for light absorption [10,11]. The incorporation of actinide elements with perovskite structure could prove to be a great deal to understand emergent properties that could lead these materials for technological applications [12][13]. In addition, it could be viable to have a computational insight into their various physical properties to guide the experiments towards more specific outcomes [14-16].

* Corresponding author: myaseen_taha@yahoo.com
https://doi.org/10.15251/DJNB.2024.192.525

Till now, various actinide series based perovskites $BaNpO_3$ [16–18], $BaAmO_3$ [7], $BaThO_3$ and $BaUO_3$ [19–21] are described as half metallic ferromagnets. Khandy *et al.* (2018) investigated the electronic and transport characteristics of $BaPaO_3$ and was regarded as potential material for micro/nano-electronics [15]. Recently, perovskites $SrPuO_3$, $SrAmO_3$ and $BaCfO_3$ were characterized for their electronic and thermoelectric features [22–24]. Actinium (Ac) based materials are has chemistry closely follows that of lanthanum [25-29]. Lanthanum (La) based perovskites are being extensively explored. While, with no qualitative difference, actinium-based materials remained still unexplored, however, the ionic radii-related quantitative differences are the only ones that exist. This makes La as a perfect surrogate for Ac elements in order to compare or analyze properties of these materials [30]. $LaAlO_3$, a widely studied polar perovskite is regarded as semiconductive nature with a DFT calculated indirect bandgap of 3.46 eV [31]. Emergence of half metallic ferromagnetism in cubic $NdGaO_3$ was observed by Monir *et al.* with 100% spin polarized 4*f*-Nd states contributing the most at the Fermi level [32]. Moreover, $LaGaO_3$ reportedly, crystalizes into orthorhombic structure having 3.14 eV band gap.

In this paper, a systematic DFT based investigation of optoelectronic and thermodynamic characteristics of ideally cubic $AcAlO_3$ and $AcGaO_3$ perovskite oxides is presented. Both proposed compounds are found to be stable in non-magnetic phase, while retaining the exceptional electronic (wide band gap), optical (high dielectric constant) and temperature-dependent transport properties. To best of our knowledge, there is not any experimental or theoretical work on these compounds published prior to this study.

2. Method of calculation

The proposed perovskites $AcAlO_3$ and $AcGaO_3$, ideally, have stable cubic structural symmetry having Pm-3m space group. In the structure, Ac, Al/Ga and O atoms were positioned at (0, 0, 0), (½, ½, ½) and (0, ½, ½), respectively. The internal atomic positions were then fully relaxed and optimized excluding the spin polarization (due to non-magnetic nature). The optimized crystal structures of both studied perovskites are displayed in Fig. 1 (b&e).

Presented physical properties of $AcXO_3$ (X = Al, Ga) are computed by solving Kohn-Sham equations [33]. Ground-state energies and geometry optimizations for both perovskites are computed by condensing the lattice parameters within the self-consistent DFT based FP-LAPW method as employed in WIEN2k code [34]. The Kohn-Sham equation is given as:

$$\left[-\frac{h^2}{2m}\nabla^2 + V_{eff}(r)\right]\phi_i(r) = \varepsilon_i\phi_i(r) \tag{1}$$

Where $-\frac{h^2}{2m}\nabla^2$ represent the kinetic energy, $V_{eff}(r)$ stands for effective potential and $\phi_i(r)$ is for Kohn-Sham orbitals. The value of $V_{eff}(r)$ is calculated by using following expression:

$$V_{eff}(r) = V_{ext} + e^2 \int \frac{\rho(r)}{r-r'}dr' + \frac{\delta_{E_{XC}}}{\delta\rho(r)} \tag{2}$$

In this equation, V_{ext} represents the electron-nucleus interactions, second term corresponds to e^-–e^- interactions named as Hartree potential and last term corresponds to the exchange correlation potential. DFT can deliver precisely calculated energies and related properties if E_{XC} is known. However, we have to approximate the E_{XC} [33,35,36]. Therefore, to estimate E_{XC}, Perdew-Burke-Ernzerhof for solids plus generalized-gradient-approximation (PBEsol + GGA) was employed [37]. The convergence of basis set was controlled by the wave function expansion. For this purpose, the plane wave cutoff parameter $R_{MT}\times K_{MAX} = 7$ was chosen. Here, R_{MT} represents the smallest value of muffin tin radius, and K_{MAX} is the maximum value of wave vector. A denser mesh of *k*-points (10×10×10) was selected to perform the Brillion zone (BZ) integration. The energy convergence criterion was selected 10^{-4} Ry and the difference of integrated charge density was chosen as $< 10^{-4}$ e/a.u.^{3}. The maximum value of angular momentum (l_{Max}) was selected as constant for outside while a maximum value of l_{Max} was set as 10 for inside the sphere for wave function.

Further, the temperature dependent transport characteristics were calculated by using the BoltzTraP code which is based on Boltzmann's semiclassical transport theory [38]. The value of constant relaxation time approximation was set as $\tau = 5\times10^{-15}$ s. The equations involved in computing the different physical characteristics are stated explicitly in the subsequent sections.

3. Results and discussions

3.1. Thermodynamical stability

Thermodynamical stabilities of the compounds under investigation are briefly discussed here and are compared with the related literature. The formula for formation enthalpies (ΔH_F) of $AcXO_3$ (X = Al, Ga) is given as under:

$$\Delta H_F = E_{Ac(Al/Ga)O_3} - E_{Ac} - E_{Al/Ga} - 3E_O \tag{3}$$

Here, E stands for total energy of respective compound or elements. From the perspective of calculated enthalpies, both compounds are found to be stable thermodynamically with ΔH_F value of –7.6799 eV for $AcAlO_3$ and –6.992 eV for $AcGaO_3$. This thermodynamical stability can be verified by comparing the $AcAlO_3$ and $AcGaO_3$ thermodynamics with Ac_2O_3 which has been synthesized experimentally in various studied [25-29]. Also, $AcCrO_3$ and $AcFeO_3$ has been computationally explored by Munir *et al*. and reported the thermodynamic stability of relevant compounds [39].

3.2. Structural stability

Structural characteristics have a critical role in forecasting the ground state phase along with atomic occupancy at various Pm-3m lattice positions and depict the bonding nature. Our proposed compounds $AcXO_3$ (X = Al, Ga) are ideally cubic with Pm-3m space group (see Fig. 1(e&b)). Brich Murnaghan's equation of state [40] was solved in order to compute ground states energies of cubic $AcXO_3$ (X = Al, Ga) in nonmagnetic (NM) and ferromagnetic (FM) phases to determine the stable phase. The Brich Murnaghan's equation is mathematically expressed as:

$$E(V) = E_O + \frac{9V_OB_O}{16}\left\{\left[\left(\frac{V_O}{V}\right)^{\frac{2}{3}} - 1\right]^3 B_0' + \left[\left(\frac{V_O}{V}\right)^{\frac{2}{3}} - 1\right]^2 - \left[6 - 4\left(\frac{V_O}{V}\right)^{\frac{2}{3}}\right]\right\} \tag{4}$$

In this equation, V and V_0 represent the thermodynamic and equilibrium volumes, respectively, B_0 is bulk modulus and B_0' is the value of its pressure derivative and E_0 is the equilibrium energy. It is observed that optimized cubic structures of both compounds have least energy (stable) in nonmagnetic phase (see Fig. 1).

Furthermore, cubic stability can be determined by computing the Goldschmidt's tolerance factor (τ_G), formula of which is given below [41]:

$$\tau_G = \frac{r_A + r_0}{\sqrt{2}(r_X + r_0)} \tag{5}$$

Here, r is respective ionic radii. The calculated τ_G values of $AcAlO_3$ and $AcGaO_3$ are 0.93 and 0.90, respectively. Governed by these theoretically predicted tolerance factors, both titled perovskite materials are found to be stable in cubic configuration with the value of τ_G approaching to unity [41]. Several other structural parameters like lattice constants a_0 in (Å), equilibrium volumes V_0 in $(a.u.)^3$, B_0 in GPa, its pressure derivative B_0', and ground state energies E_0 in Ryd. are reported in Table 1.

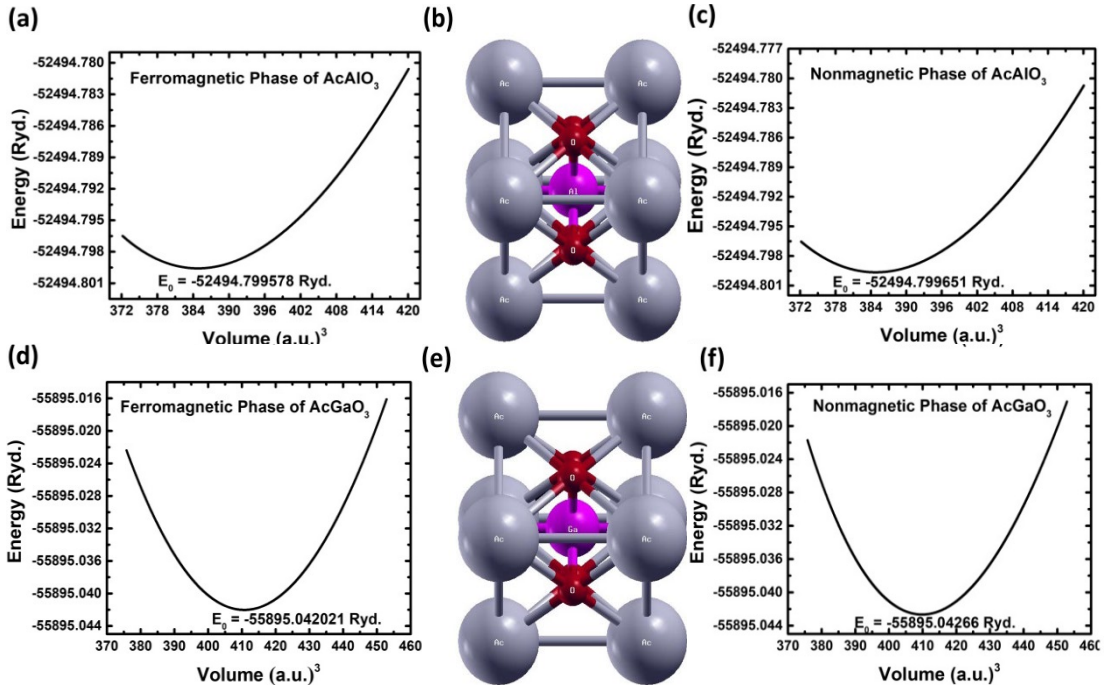

Fig. 1. The optimized energy vs volume (E-V) curve for (a, d) ferromagnetic phase (left side), (c, f) nonmagnetic phase (right side) and (b, e) optimized Pm-3m crystal structure (middle panel) of $AcAlO_3$ and $AcGaO_3$.

Table 1. Ground state parameters, formation enthalpy ΔH_f, and tolerance factor τ_G of studied $AcAlO_3$ and $AcGaO_3$ perovskites.

Crystals	**$AcAlO_3$**	**$AcGaO_3$**
Lattice constant a_0, (Å)	3.8489	3.9334
Volume V_0, $(a.u.)^3$	384.7890	410.6906
B_0, (GPa)	205.6313	187.2768
B_0'	5.0	0.6285
E_O, (eV)	–52494.799578	–55895.042021
ΔH (eV)	–7.6799	–6.992
Tolerance factor, τ_G	0.93	0.90

3.3. Electronic structures and density of states

Electronic band structures (BS) of materials elucidate a fundamental explanation of material's electrical properties. In this section of results and discussions, we have discussed the BSs of $AcAlO_3$ and $AcGaO_3$ calculated along highly symmetric directions of BZ within PBE+GGA scheme. It can be seen from the calculated BSs (see Fig. 2) that $AcAlO_3$ has direct band gap while $AcGaO_3$ has indirect band gap. The numerical values of bandgaps (E_g) calculated for $AcAlO_3$ and $AcGaO_3$ by PBE+GGA are 3.98 eV (Γ–Γ) and 2.75 eV (R–Γ), respectively, and are also tabulated in Table 2.

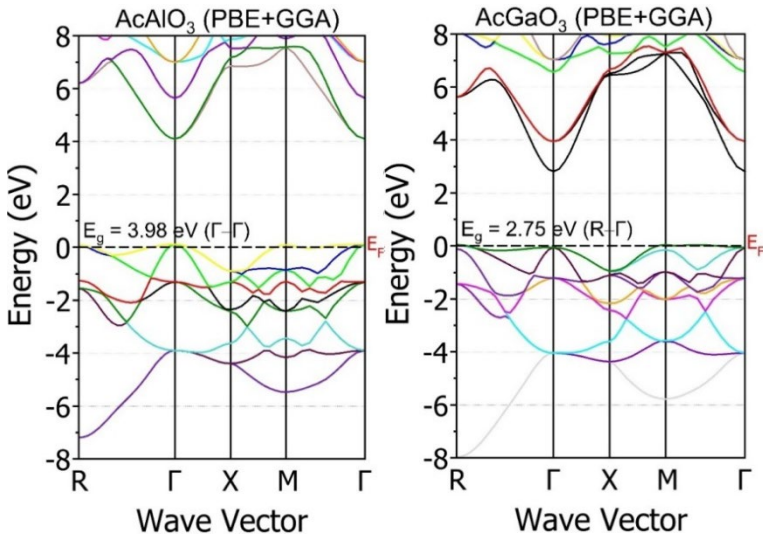

Fig. 2. The electronic band structures of $AcAlO_3$ (left) and $AcGaO_3$ (right) along with R-Γ-X-M-Γ direction of BZ.

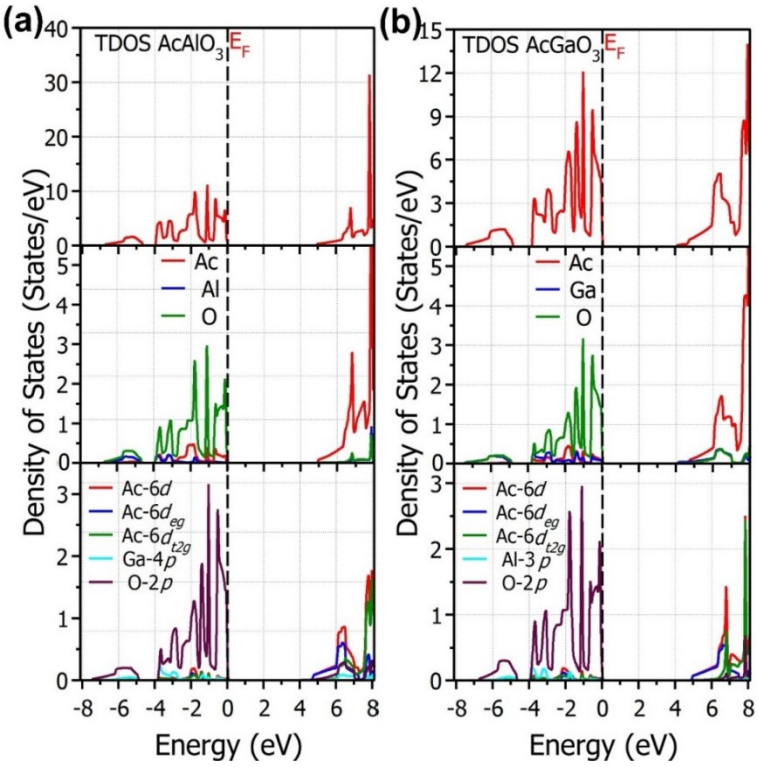

Fig. 3. The electronic density of states (TDOS: top, TDOS of atoms: middle, PDOS: bottom) of (a); $AcAlO_3$ and (b); $AcGaO_3$.

This reduction of band gap after Ga substitution at Al site in MO_6 octahedra is due to the greater ionic radii of Ga than Al, which eventually lead to less coulomb repulsion resulting in low band gap. For the deeper insight into the electronic properties, the total (T), atomic total DOS and contribution of partially filled Ac-6*d*, Al-3*p*/Ga-4*p*, and O-2*p* valence states towards the band alignment are computed (see Fig. 3). Among all states, most interesting states are 6*d*/2*p* of Ac/O atoms which lie in vicinity of Fermi level (E_F). Coulomb repulsion among electrons of Ac with nearby atoms making the case for degeneracy of *d*-orbitals that are split into doublet *d*-e_g (d_x^2-

$_y^2$,d_z^2) states at lower energy and triplet d-t_{2g} (d_{xy},d_{yz},d_{zx}) states pushed towards higher energy. Oxygen, the most electro-negative constituent atom in both titled perovskite oxide systems gain electrons from all metals and hence have maximum contribution in valence band (VB) formation (see Fig. 3). The obtained results of electronic states of nonmagnetic $AcXO_3$ (X = Al, Ga) are similar to the electronic profiles of recently reported $BaPaO_3$, $BaUO_3$ [42,43], $BaNpO_3$ [16] perovskites.

3.3. Optical spectra

The energy levels of the ground state gradually perturb over incident light, and optical transitions between the occupied and unoccupied states are investigated to describe the interaction of electron with incident photon. Motivated by the prospect of their application in optoelectronic devices, the BS dependent optical properties of titled single perovskite oxides are explored. Frequency (ω) dependent complex dielectric function (DF) is calculated, through which all other optical parameters are extracted. The dielectric tensor Ɛ(ω) describes the polarizability of a material, relating the shape of the VB charge density, and demonstrates the deformability of the electronic contribution. The optical characteristics of a material are predicted by calculating complex dielectric function, which is comprised of two parts, real part $Ɛ_1(ω)$ and imaginary part $Ɛ_2(ω)$ and are expressed in a relation given below [44]:

$$Ɛ(\omega) = Ɛ_1(\omega) + iƐ_2(\omega) \tag{6}$$

The imaginary part $Ɛ_2(ω)$ which arises form intra and inter band transitions, depicts the probable transitions between occupied and unoccupied energy levels using fixed k-vector over Brillouin zone (BZ). It is mainly due to the inter-band transitions, rather than intra-band changes, that contribute more to the semiconductors. The $Ɛ_2(ω)$ is mathematically defined as [45]:

$$Ɛ_2(\omega) = \frac{e^2\hbar}{\pi m^2\omega^2}\sum_{vc}\int |n, n'(k,q)|^2\, \delta\left[\omega_{n,ń}(k) - \omega\right] d^3k` \tag{7}$$

where q and k denote the wave functions of occupied and unoccupied states, and the first term inside the integration indicates the normalization of momentum matrix element. The real part of dielectric function $Ɛ_1(ω)$ elucidates the polarization of light and can be computed via Kramers-Kronig relationship which is given as under [46]:

$$Ɛ_1(\omega) = 1 + \frac{2}{\pi}p\int_0^{\theta}\frac{\omega' Ɛ_2(\omega')}{\omega'^2-\omega^2}d\omega' \tag{8}$$

where, p is the integral's principal value.

The $Ɛ_1(ω)$ and $Ɛ_2(ω)$ plots (see Fig. 4a&b) show the cut off value $Ɛ_1(ω)$ of 4.0 for $AcAlO_3$ and 4.2 for $AcGaO_3$ and turns to peak values of 9.1 at 6.75 eV for $AcAlO_3$ and 9.35 at 6.15 eV for $AcGaO_3$. Above this energy limit, a dip to the negative values is obtained in the corresponding energy ranges of 9 to 9.8 eV for $AcAlO_3$ while $AcGaO_3$ remains negative from 9.0 eV to onward (see Fig. 4a & b). These negative $Ɛ_1(ω)$ values show metallic character of the studied perovskites within corresponding photon energy ranges. The $Ɛ_2(ω)$ plots for $AcAlO_3$ indicate that maximum peaks lie within the energy range of 7–10 eV with an onset of saturation edge recorded at 4.2 eV. While with an onset of the first $Ɛ_2(ω)$ peak edge at 4 eV, the $AcGaO_3$ compound show highest imaginary part within 6.2 to 9 eV energy range. Afterwards, both perovskites show considerable variation towards minimum $Ɛ_2(ω)$ value.

The optical absorption α(ω) and optical conductivity σ(ω) can be deducted from Ɛ(ω) and the formulas for both properties are given below [45]:

$$\alpha(\omega) = \sqrt{2\omega}\left(\sqrt{[Ɛ_1^2(\omega) + Ɛ_2^2(\omega)]} - Ɛ_1(\omega)\right)^{\frac{1}{2}} \tag{9}$$

$$\sigma(\omega) = \frac{\omega}{4\pi}Ɛ_2(\omega) \tag{10}$$

Fig. 4c shows α(ω) plots which is basically the measure of attenuation percentage for intensity of incident photons that is absorbed per unit length in studied oxides. The pattern of α(ω) plot is relatively similar to that of $\varepsilon_2(\omega)$ plot (see Fig. 4a,b&c) for both Al and Ga based perovskites. Hence, α(ω) is also related to the presented BSs of both compounds. The onset edge of absorption spectra is at 5 eV for $AcAlO_3$ and 4 eV for $AcGaO_3$.

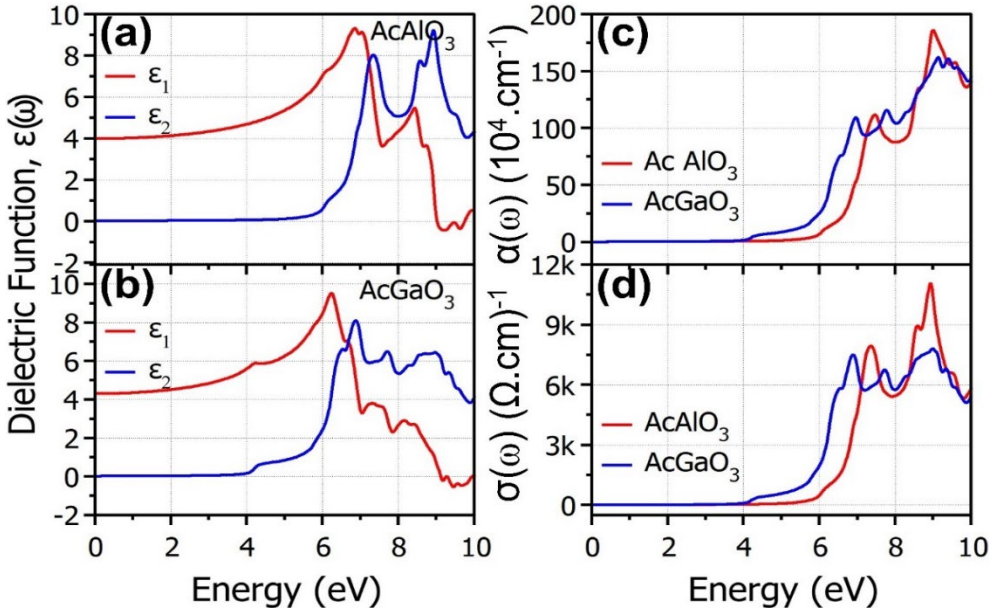

Fig. 4. (a & b); $\varepsilon_1(\omega)$ and $\varepsilon_2(\omega)$ (right panel), (c); α(ω), and (d); σ(ω) for $AcAlO_3$ and $AcGaO_3$.

At lower energies, from 0 eV to onset edge, there is zero or negligible absorption, meaning that material is transparent to the incident light with the energy of this range (reflectivity is also minimum in this range as discussed below). The maximum α(ω) peaks are observed in 7–10 eV energy range for considered oxides. The highest absorption is obtained at 9 eV with $\alpha = 180\times10^4$ cm^{-1} for $AcAlO_3$ and $\alpha = 170\times10^4$ cm^{-1} for $AcGaO_3$. When light of particular frequency interacts with a material, its electrons gain energy and jump to CB. These free charge carriers make the material conductive for which optical conductivity σ(ω) term is used. The onset edges of calculated σ(ω) (see Fig. 4d) are observed at 4.5 and 4.0 eV energy for Al and Ga based perovskites, correspondingly. The first maximum σ(ω) peaks have the values of 7650 (at 7.1 eV) and 7680 $\Omega^{-1}cm^{-1}$ (at 6.7 eV) for $AcAlO_3$ and $AcGaO_3$, respectively. This conductivity arises along the highly symmetric (Γ–Γ) direction of the BZ for $AcAlO_3$, while (R–Γ) direction of first BZ for $AcGaO_3$. The maximum optical conductivity occurs with a value of 11000 $\Omega^{-1}cm^{-1}$ at 8.9 eV for $AcAlO_3$ and 7800 $\Omega^{-1}cm^{-1}$ at 9.0 eV for $AcGaO_3$ followed by decrement afterwards. This interplay of EM interaction with material and resulted transitions from valence band to conduction band are well correlated with shapes of band structures of studied oxides.

Other significant optical characteristics, such as the n(ω), and k(ω), may be obtained using $\varepsilon_1(\omega)$ and $\varepsilon_2(\omega)$ [45].

$$n(\omega) = \frac{1}{\sqrt{2}}\left(\sqrt{[\varepsilon_1^2(\omega) + \varepsilon_2^2(\omega)]} + \varepsilon_1(\omega)\right)^{\frac{1}{2}} \tag{11}$$

$$k(\omega) = \frac{1}{\sqrt{2}}\left(\sqrt{[\varepsilon_1^2(\omega) + \varepsilon_2^2(\omega)]} - \varepsilon_1(\omega)\right)^{\frac{1}{2}} \tag{12}$$

Generally, the relationship between propagation of EM wave through vacuum and in materials can be mathematically expressed as: N(ω) = n(ω) + *i*k(ω). An analytical glance on *n*(ω) plot (Fig. 5a) revealed the static n(0) value of 2.0 and 2.1 for $AcAlO_3$ and $AcGaO_3$ perovskites,

respectively. The calculated static values of $n(\omega)$ satisfy the following optical relation $n^2(0)=\varepsilon_1(0)$. The $n(\omega)$ plot for both compounds have pattern similar to that of real part of DF, i.e., $\varepsilon_1(\omega)$ (see Figs. 5a & 4c). The principal peak value of $n(\omega)$ recorded for $AcAlO_3$ is 3.3 at 7 eV and for $AcGaO_3$ is 3.2 at 6.2 eV. Thereafter, the $n(\omega)$ plot shows a fluctuated dip all the way towards 10 eV with lowest value of ~1 at 10 eV for both oxides.

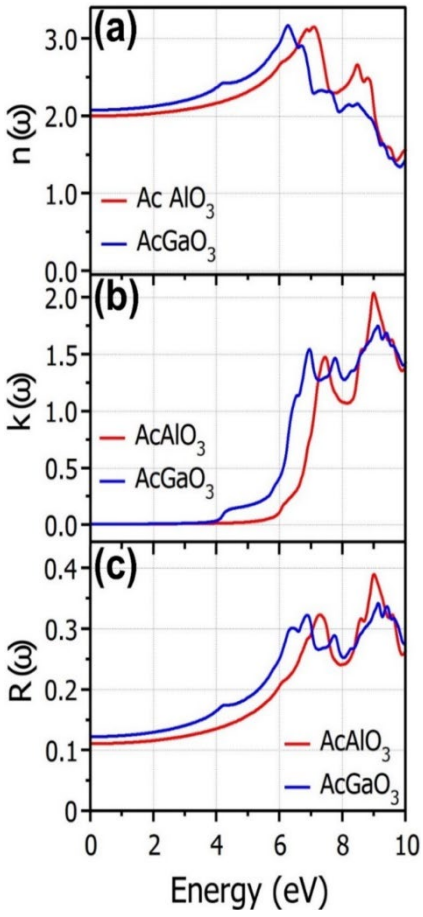

Fig. 5. (a) n(ω), (b); k(ω), (c); R(ω) for $AcAlO_3$ and $AcGaO_3$.

From the $k(\omega)$ spectra (Fig. 5b), it is clear that nature of $k(\omega)$ peaks is analogous to that of $\varepsilon_2(\omega)$. The onset edges of $k(\omega)$ peaks are similar as that of $\varepsilon_2(\omega)$, $\alpha(\omega)$, and $\sigma(\omega)$. The first maximum peak value of $k(\omega)$ observed for $AcAlO_3$ is 1.49 at 7.2 and 1.55 at 7 eV for $AcGaO_3$. The trend in $k(\omega)$ fluctuation is similar to that of $\varepsilon_2(\omega)$ peaks.

To further understand the response of studied perovskites to incident light, reflectivity $R(\omega)$ in terms of percentage is also calculated for $AcXO_3$ (X = Al, Ga) compounds by using following formula:

$$R(\omega) = \frac{[n(\omega)-1]^2 + k^2(\omega)}{[n(\omega)+1]^2 + k^2(\omega)} \tag{13}$$

From the Fig. 5c, we can realize that $R(\omega)$ values for $AcXO_3$ (X = Al, Ga) at 0 eV are 11% and 12.5%, respectively. From 0 to 4.0 eV, the reflection of incident light is negligible. In this energy range, the $\alpha(\omega)$ for studied perovskites are of the order of 10^4 cm^{-1} while reflection is less than 15%. Clearly, this comparison of the absorption and reflectivity curves in the above-mentioned range shows that incoming photons of this energy range are mostly transferred. The similar transparent character of actinide series-based perovskite oxides has been interpreted

similarly in Ref. [47]. Moreover, Table 2 also enlists the cutoff values of various optical parameters i.e., Ɛ(0), *n*(0) and R(0).

Table 2. PBE+GGA calculated electronic band gap E_g (eV) and cut off values of various optical parameters for both $AcAlO_3$ and $AcGaO_3$ perovskite oxides.

Perovskites	Band Gap, E_g (eV)	Optical Parameters		
	GGA	$Ɛ_1(0)$	*n*(0)	R(0)
$AcAlO_3$	3.98 (Γ–Γ)	4.0	2.0	11%
$AcGaO_3$	2.75 (R–Γ)	4.2	2.1	12.5%

3.4. Thermoelectric (TE) response

As a result of the serious environmental changes, organic energy resources are diminishing or decreasing, posing a significant danger to sustainable living. This demands the exploration for novel materials to eliminate such kind of challenges. The scientific community is extensively working to identify the particular alternative resources that are pollution free, financially viable, and highly efficient. It was recently suggested that increase in TE efficiency of a material is dependent on quantum confinement of charge carriers [48]. Inspired by this suggestion, researchers used half Heusler alloys together with silicides, clathrates, and skutterudites in an attempt to solve these problems [49]. The shortcomings of such material's instability at high temperatures and rarity in abundance make them impractical for widespread commercialization. In this regard, TE oxides are anticipated to overcome these obstacles [12,50–54]. Here, in an attempt to forecast TE characteristics of $AcAlO_3$ and $AcGaO_3$, semiclassical transport theory of Boltzmann was utilized along with constant relaxation time and rigid body approximation as integrated in BoltzTraP code [38]. The theory is quite helpful for comprehending different transport coefficients including Seebeck coefficient (*S*), electrical and thermal conductivities (σ/τ & κ/τ), associated power factor (PF), and figure of merit (ZT).

In order to better understand how waste energy is transformed into usable energy, these coefficients have been thoroughly evaluated. For $AcAlO_3$, the value of σ/τ rises with the upsurge in temperature (see Fig. 6a). It is reported that semiconductor materials have negative temperature coefficient, i.e., their resistance decreases with the linear increase in temperature [55]. While electrical conductivity (σ/τ) for $AcGaO_3$ is low at higher temperatures might be due to indirect transition. The maximum σ/τ for $AcAlO_3$ is observed within 450 – 800 K temperature range. However, for $AcGaO_3$, the maximum σ/τ is observed at 200 K and it is lowest at 800 K. The thermal energy is transferred by two mechanisms: first, holes and second, electron drift, which contribute the electronic thermal conductivity (κ_e) while phonon's traveling contributes the lattice thermal conductivity (κ_l), both parts are related as $\kappa = \kappa_e + \kappa_l$. However, only κ_e are computed due to low contribution of lattice conductivity at high temperature (see Fig. 6b). An increasing trend for $AcAlO_3$ and $AGaO_3$ is observed with highest κ_e values of 25×10^{14} and 25.2×10^{14} W/cm.K.s., respectively at 800 K.

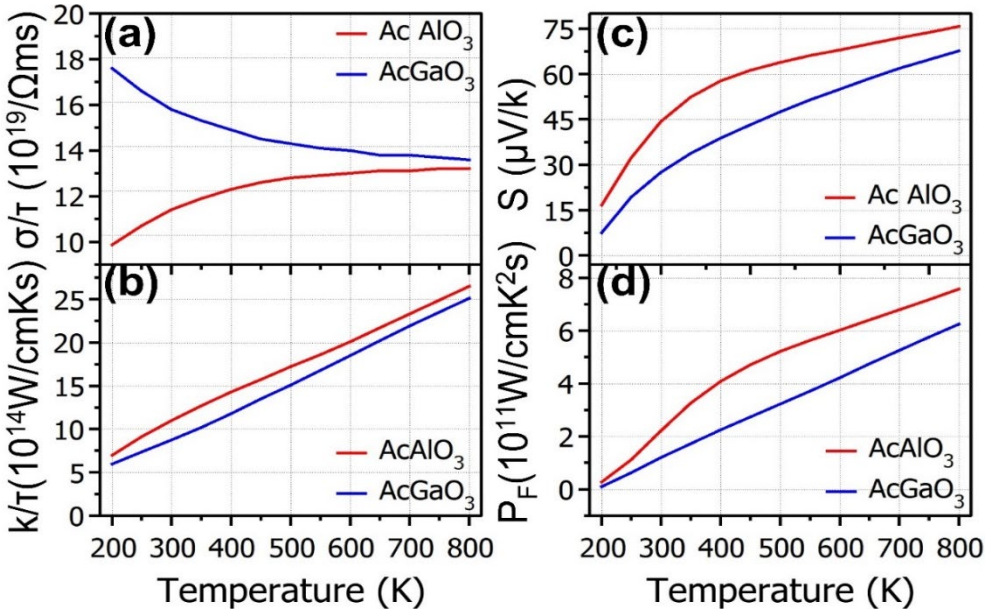

Fig. 6. (a); electrical conductivity, (σ/τ in 10^{19} $\Omega^{-1}ms$), (b); electronic thermal conductivity, (κ_e/τ in 10^{14} $WK^{-1}m^{-1}$), (c);S in $\mu V/k$, and (d);PF in 10^{11} $Wm^{-1}K^{-2}m^{-1}$ of $AcAlO_3$ and $AcGaO_3$.

A single type of carriers—either p-type or n-type—should be used to assure high thermopower since multiple types of carriers cancel each other out and produce lower potential [56]. By calculating the seebeck coefficient (S), one may determine a material's thermopower, and S can be computed as follows:

$$S = \frac{8\pi^2 k^2 1}{3e\hbar^2} m^* T \left(\frac{\pi}{3n}\right)^{\frac{2}{3}} \tag{14}$$

Hence, S and effective mass (m*) are directly proportional to each other. The magnitude of the thermoelectric voltage produced by a temperature gradient between two ends of a material is expressed in terms of the seebeck coefficient. For efficient TE material, the *S* value should be high. The value of *S* increases sharply at low temperatures for both compounds, however, the slopes become smaller at higher temperatures (see Fig. 6c). $AcAlO_3$ retains comparatively high *S* values than $AcGaO_3$ throughout the whole 200–800 K temperature range.

Further, power factor PF of $AcAlO_3$ and $AcGaO_3$ is investigated (see Fig. 6d) which is calculated by using the formula $PF=S^2\sigma$. At 800 K, the PF reaches to its maximum value of 7.5×10^{11} and 6.2×10^{11} W/cm.K^2.s. for $AcAlO_3$ and $AcGaO_3$, respectively. For all the temperature range of 200–800 K, $AcAlO_3$ has higher PF as compared to $AcGaO_3$. This behaviour could be due to higher value of *S*.

The efficiency of TE materials depends on ZT, also termed as the figure of merit, and is enumerated using following formula:

$$ZT = \frac{S^2\sigma}{k_e} T \tag{15}$$

The resultant ZT quantity is unit less. From the Fig. 7, a linearly up surging trend is observed for both proposed oxides within 200 to 800 K. At 800 K, the recorded ZT for $AcAlO_3$ and $AcGaO_3$ are 0.23 and 0.20, respectively. This trend is in line with the σ/τ, κ_e, and *S* calculated for both titled perovskites as presented in Fig. 6.

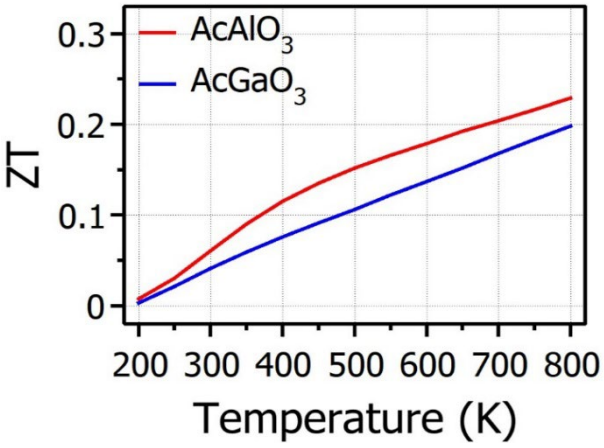

Fig. 7. Figure of merit, (ZT) of $AcAlO_3$ and $AcGaO_3$.

4. Conclusions

We have employed FP-LAPW method which is based on DFT to examine and predict the physical characteristics of $AcAlO_3$ and $AcGaO_3$ perovskites. The PBE-GGA has been utilized to estimate the band gaps. The calculated band gap values are 3.98 for $AcAlO_3$ and 2.75 eV for $AcGaO_3$. Optical parameters including absorption coefficient and optical conductivity are also calculated to shed the light on the optical response of the studied materials. Furthermore, temperature dependent transport properties have been explored. Based on presented results, both $AcAlO_3$ and $AcGaO_3$ are found to be good UV absorbers and are regarded as potential candidate for UV based electronics and thermoelectric devices.

Acknowledgements

The authors extend their appreciation to the Research Centre for Advanced Materials Science (RCAMS), King Khalid University, Saudi Arabia, for funding this work under grant number RCAMS/KKU/011-22. The authors also express their gratitude to Princess Nourah bint Abdulrahman University Researchers Supporting Project number (PNURSP2024R81), Princess Nourah bint Abdulrahman University, Riyadh , Saudi Arabia.

References

[1] M. Hamid Elsheikh, D. A. Shnawah, M. F. M. Sabri, S. B. M. Said, M. Haji Hassan, M. B. Ali Bashir, M. Mohamad, Renew. Sustain. Energy Rev. 30, 337 (2014); https://doi.org/10.1016/j.rser.2013.10.027

[2] R. Liu, J. Duay, S. B. Lee, ACS Nano 4, 4299 (2010); https://doi.org/10.1021/nn1010182

[3] V.-H. Nguyen, H. Do, N. van Tuan, P. Singh, P. Raizada, A. Sharma, S.S. Sana, A. Grace, M. Shokouhimehr, S.H. Ahn, C. Xia, S.Y. Kim, Q. Le, Solar Energy 211, 584 (2020); https://doi.org/10.1016/j.solener.2020.09.078

[4] R. Haunschild, A. Barth, B. French, J Cheminform 11, 72 (2019); https://doi.org/10.1186/s13321-019-0395-y

[5] M. Nazar, Nasarullah, S. A. Aldaghfag, M. Yaseen, M. Ishfaq, R. A. Khera, S. Noreen, M. H. Abdellattif, Journal of Physics and Chemistry of Solids 166, 110719 (2022); https://doi.org/10.1016/j.jpcs.2022.110719

[6] G. L. Murphy, B. J. Kennedy, Z. Zhang, M. Avdeev, H. E. A. Brand, P. Kegler, E. V. Alekseev, J Alloys Compd 727, 1044 (2017); https://doi.org/10.1016/j.jallcom.2017.08.200

[7] S. A. Dar, V. Srivastava, U. K. Sakalle, S. Ahmad Khandy, D. C. Gupta, J Supercond Nov Magn 31, 141 (2018); https://doi.org/10.1007/s10948-017-4181-7

[8] M. I. Hussain, R. M. A. Khalil, F. Hussain, A. M. Rana, Int J Energy Res 45, 2753 (2021); https://doi.org/10.1002/er.5968

[9] A. Sohail, S. A. Aldaghfag, M. KButt, M. Zahid, J. Iqbal, M. Ishfaq, A. Dahshan, Journal of Ovonic Research 17, 461 (2021).

[10] Hayatullah, G. Murtaza, R. Khenata, S. Mohammad, S. Naeem, M. N. Khalid, A. Manzar, Physica B Condens Matter 420, 15 (2013); https://doi.org/10.1016/j.physb.2013.03.011

[11] Hayatullah, G. Murtaza, R. Khenata, S. Muhammad, A. H. Reshak, K. M. Wong, S. Bin Omran, Z. A. Alahmed, Comput Mater Sci 85, 402 (2014); https://doi.org/10.1016/j.commatsci.2013.12.054

[12] M. Nabi, T. M. Bhat, D. C. Gupta, J Supercond Nov Magn 32, 1751 (2019); https://doi.org/10.1007/s10948-018-4872-8

[13] G. L. Murphy, B. J. Kennedy, Z. Zhang, M. Avdeev, H. E. A. Brand, P. Kegler, E. V. Alekseev, J Alloys Compd 727, 1044 (2017); https://doi.org/10.1016/j.jallcom.2017.08.200

[14] S. Ahmad Dar, V. Srivastava, U. Kumar Sakalle, V. Parey, J Electron Mater 47, 3809 (2018); https://doi.org/10.1007/s11664-018-6251-4

[15] S. A. Khandy, I. Islam, D. C. Gupta, A. Laref, J Mol Model 24, 1 (2018); https://doi.org/10.1007/s00894-018-3666-z

[16] S. A. Khandy, D. C. Gupta, Structural, Mater. Chem. Phys. 198, 380 (2017); https://doi.org/10.1016/j.matchemphys.2017.06.033

[17] S. A. Khandy, D. C. Gupta, J. Electron. Mater. 46, 5531 (2017); https://doi.org/10.1007/s11664-017-5620-8

[18] S. A. Dar, S. A. Khandy, I. Islam, D. C. Gupta, U. K. Sakalle, V. Srivastava, K. Parrey, Chin. J. Phys. 55, 1769 (2017); https://doi.org/10.1016/j.cjph.2017.08.002

[19] F. Shakoor, S. A. Aldaghfag, M. Yaseen, M. K. Butt, S. Mubashir, J. Iqbal, M. Zahid, A. Murtaza, A. Dahshan, Chem Phys Lett 779, 138835 (2021); https://doi.org/10.1016/j.cplett.2021.138835

[20] Z. Ali, I. Ahmad, A. H. Reshak, Physica B 410, 217 (2013); https://doi.org/10.1016/j.physb.2012.11.008

[21] K. Kurosaki, T. Matsuda, M. Uno, S. ichi Kobayashi, S. Yamanaka, J Alloys Compd 319, 271 (2001); https://doi.org/10.1016/S0925-8388(01)00876-3

[22] S. A. Dar, V. Srivastava, U. K. Sakalle, A. Rashid, G. Pagare, Mater Res Express 5, 026106 (2018); https://doi.org/10.1088/2053-1591/aaabcd

[23] S. A. Dar, V. Srivastava, U. K. Sakalle, J Supercond Nov Magn 30, 3055 (2017); https://doi.org/10.1007/s10948-017-4155-9

[24] S. A. Khandy, I. Islam, D. C. Gupta, R. Khenata, A. Laref, S. Rubab, Mater Res Express 5, 105702 (2018); https://doi.org/10.1088/2053-1591/aad9eb

[25] E. V. Shkol'Nikov, Russian Journal of Applied Chemistry 82, 2098 (2009); https://doi.org/10.1134/S1070427209120040

[26] James G. Reavis, Experimental Studies of Actinides in Molten Salts, Los Alamos National Lab., New Maxico, USA, 1985; https://doi.org/10.2172/5492312

[27] W. D. Shults, Analytical Chemistry Division Progress Report, Oak Ridge, Tennessee, 1981.

[28] R. J. M. Konings, L. R. Morss, J. Fuger, Thermodynamic Properties of Actinides and Actinide Compounds, in: The Chemistry of the Actinide and Transactinide Elements, 3rd ed., Vol. 4, Springer, Dordrecht, 2113-2224 (2008); https://doi.org/10.1007/1-4020-3598-5_19

[29] R. A. Lidin, V. A. Molochko, L. L. Andreeva, Reactivity of Inorganic Substances: Revised and Augmented Edition, Begell House Inc., New York, 1996; https://doi.org/10.1615/978-1-56700-050-4.0

[30] H. W. Kirby and L. R. Morss, Actinium, in: The Chemistry of the Actinide and Transactinide Elements, 3rd ed., Vol. 2, Springer, Dordrecht, 18-51 (2008); https://doi.org/10.1007/1-4020-3598-5_2

[31] M. Yaseen, A. Ashfaq, A. Akhtar, R. Asghar, H. Ambreen, M.K. Butt, S. Noreen, S. Ur Rehman, S. Bibi, S.M. Ramay, A. Murtaza, Mater Res Express 7, 015907 (2019); https://doi.org/10.1088/2053-1591/ab6110

[32] M. El Amine Monir, H. Baltach, F. El Haj Hassan, A. Bahnes, Z. Bahnes, J Supercond Nov Magn 32, 2149 (2019); https://doi.org/10.1007/s10948-018-4938-7

[33] W. Kohn, L. J. Sham, Physical Review 140, A1133 (1965); https://doi.org/10.1103/PhysRev.140.A1133

[34] Peter Blaha, Karlheinz Schwarz, Georg Madsen, Dieter Kvasnicka, and Joachim Luitz, WIEN2k: An Augmented Plane Wave Plus Local Orbitals Program for Calculating Crystal Properties, User's Guide, Vol. 1, Techn. Universitat Wien, Vienna, (2011).

[35] H. Shafique, S. A. Aldaghfag, M. Kashif, M. Zahid, M. Yaseen, J. Iqbal , R. Neffati, Chalcogenide Letters, 18(10), 589 - 599 (2021).

[36] A. J. Cohen, P. Mori-Sánchez, W. Yang, J Chem Phys 126, 191109 (2007); https://doi.org/10.1063/1.2741248

[37] J. P. Perdew, K. Burke, M. Ernzerhof, Phys. Rev. Lett. 77, 3865 (1996); https://doi.org/10.1103/PhysRevLett.77.3865

[38] G. K. H. Madsen, D. J. Singh, Comput Phys Commun 175, 67 (2006); https://doi.org/10.1016/j.cpc.2006.03.007

[39] J. Munir, M. K. Iftikhar, M. I. Jamil, M. U. Din, T. Alshahrani, H. I. Elsaeedy, Q. Ain, Phys Scr 98, 065513 (2023); https://doi.org/10.1088/1402-4896/accf4a

[40] V. Tyuterev, N. Vast, Comput Mater Sci 38, 350 (2006); https://doi.org/10.1016/j.commatsci.2005.08.012

[41] T. Sato, S. Takagi, S. Deledda, B. C. Hauback, S. I. Orimo, Sci Rep 6, 23592 (2016); https://doi.org/10.1038/srep23592

[42] M. Lal, S. Kapila, International Journal of Pure and Applied Physics 13, 67 (2017).

[43] N. Erum, M. A. Iqbal, Materials Research Express 4, 025904 (2017); https://doi.org/10.1088/2053-1591/aa5d8d

[44] D. R. Penn, Phys. Rev. 128, 2093 (1962); https://doi.org/10.1103/PhysRev.128.2093

[45] J. Sólyom, Optical Properties of Solids, in Fundamentals of the Physics of Solids, Springer, Berlin, Heidelberg, 411-447 (2009); https://doi.org/10.1007/978-3-540-85316-9_10

[46] M. W. Haakestad, J. Skaar, V. Lucarini, F. Bassani, K. Peiponen, J. J. Saarinen, Opt Express 13, 9922 (2005); https://doi.org/10.1364/OPEX.13.009922

[47] T. J. Coutts, J. D. Perkins, D. S. Ginley, T. O. Mason, Transparent Conducting Oxides: Status and Opportunities in Basic Research, in 195th Meeting of the Electrochemical Society Seattle, Washington, (1999).

[48] G. Grosso and G. P. Parravicini, Optical and Transport Properties of Metals, Solid State Physics, 2nd ed., Academic Press, 483-528 (2014); https://doi.org/10.1016/B978-0-12-385030-0.00011-6

[49] W. Xie, A. Weidenkaff, X. Tang, Q. Zhang, J. Poon, T. M. Tritt, Nanomaterials 2, 379 (2012); https://doi.org/10.3390/nano2040379

[50] A. Aziz, S. A. Aldaghfag, M. Zahid, J. Iqbal, Misbah, M. Yaseen, H. H. Somaily, Physica B Condens Matter 630, 413694 (2022); https://doi.org/10.1016/j.physb.2022.413694

[51] S. Mubashir, M. K. Butt, M. Yaseen, J. Iqbal, M. Iqbal, A. Murtaza, A. Laref, Optik (Stuttg) 239, 166694 (2021); https://doi.org/10.1016/j.ijleo.2021.166694

[52] Y. Pei, X. Shi, A. LaLonde, H. Wang, L. Chen, G. J. Snyder, Nature 473, 66 (2011); https://doi.org/10.1038/nature09996

[53] L. R. Morss, J. Fuger, H. D. B. Jenkins, J Chem Thermodyn 14, 377 (1982); https://doi.org/10.1016/0021-9614(82)90057-X

[54] M. Z. Kazim, M. Yaseen, A. Ghaffar, B. A. Ijaz, Arab. J. Sci. Eng., 48, 779 (2023); https://doi.org/10.1007/s13369-022-06985-1
[55] A. Hanif, S. A. Aldaghfag, A. Aziz, M. Yaseen, A. Murtaza, Int. J. Energy Res., (2022).
[56] A. V. da Rosa, J. C. Ordóñez, Thermoelectricity, in: Fundamentals of Renewable Energy Processes, Academic Press, Elsevier, Cambridge, Massachusetts, 187 (2022); https://doi.org/10.1016/B978-0-12-816036-7.00015-4